Mon. Not. R. Astron. Soc. **000**, 1–12 (2014) Printed 10 December 2015 (MN LATEX style file v2.2)

Growing massive black holes through super-critical accretion of stellar-mass seeds

A. Lupi[1,3], F. Haardt[1,3], M. Dotti[2,3], D.Fiacconi[4], L. Mayer[4] & P. Madau[4,5]
[1] *DiSAT, Università degli Studi dell'Insubria, Via Valleggio 11, I-22100 Como, Italy*
[2] *Dipartimento di Fisica, Università degli Studi di Milano Bicocca, Piazza della Scienza 3, I-20126 Milano, Italy*
[3] *INFN, Sezione di Milano-Bicocca, Piazza della Scienza 3, I-20126 Milano, Italy*
[4] *Center for Theoretical Astrophysics and Cosmology, Institute for Computational Science, University of Zurich, Winterthurerstrasse 190, 8057 Zurich, Switzerland*
[5] *Department of Astronomy & Astrophysics, University of California, 1156 High Street, Santa Cruz, CA 95064, USA*

arXiv:1512.02651v1 [astro-ph.GA] 8 Dec 2015

Draft 10 December 2015

ABSTRACT

The rapid assembly of the massive black holes that power the luminous quasars observed at $z \sim 6-7$ remains a puzzle. Various direct collapse models have been proposed to head-start black hole growth from initial seeds with masses $\sim 10^5 M_\odot$, which can then reach a billion solar mass while accreting at the Eddington limit. Here we propose an alternative scenario based on radiatively inefficient super-critical accretion of stellar-mass holes embedded in the gaseous circum–nuclear discs (CNDs) expected to exist in the cores of high redshift galaxies. Our sub-pc resolution hydrodynamical simulations show that stellar-mass holes orbiting within the central 100 pc of the CND bind to very high density gas clumps that arise from the fragmentation of the surrounding gas. Owing to the large reservoir of dense cold gas available, a stellar-mass black hole allowed to grow at super-Eddington rates according to the "slim disc" solution can increase its mass by 3 orders of magnitudes within a few million years. These findings are supported by simulations run with two different hydro codes, RAMSES based on the Adaptive Mesh Refinement technique and GIZMO based on a new Lagrangian Godunov-type method, and with similar, but not identical, sub-grid recipes for star formation, supernova feedback, black hole accretion and feedback. The low radiative efficiency of super-critical accretion flows are instrumental to the rapid mass growth of our black holes, as they imply modest radiative heating of the surrounding nuclear environment.

Key words: black hole - galaxy formation - galaxy evolution.

1 INTRODUCTION

Observations of luminous quasars at very high redshift pose crucial questions on the formation of massive black holes (MBHs) along the history of the Universe. The most distant quasar to date, ULAS J1120+0641, lies at redshift $z = 7.084$, and it is believed to be powered by a $\sim 2 \times 10^9\,M_\odot$ MBH (Mortlock et al. 2011) that was therefore in place (and shining) 0.76 Gyr after the Big Bang. Together with the handful of bright quasars observed by the *Sloan Digital Sky Survey* at $z \gtrsim 6$ (Fan et al. 2006), ULAS J1120+0641 sets tight constraints on any model for the formation and growth of MBHs at early epochs.

It has been long thought that the first MBH seeds were *light*, specifically $\sim 100\,M_\odot$ remnants of the first generation of stars, plausibly formed at $z \gtrsim 20$ (e.g., Madau & Rees 2001; Haiman & Loeb 2001; Heger et al. 2003; Volonteri, Haardt & Madau 2003; Madau et al. 2004). If gas accretion is Eddington-limited, light seeds could grow to the supermassive variety by $z \sim 7$ only if (i) gas accretion continued unimpeded at the Eddington rate for $\gtrsim 0.6$ Gyr, and if (ii) the mass-to-light conversion efficiency of the accretion process was not high, $\epsilon \lesssim 0.1$ (Tanaka & Haiman 2009). The first condition seems hard to satisfy in the shallow potential of low–mass dark matter haloes, as radiative feedback from the progenitor and from BH accretion itself dramatically affects the gas inflow and its supply to the hole, resulting in sub–Eddington rates, therefore negligible mass growth (e.g., Wise, Turk & Abel 2008; Milosavljević et al. 2009; Alvarez, Wise & Abel 2009). The second condition is problematic too, as it requires a radiative efficiency well below that proper of accretion onto rapidly rotating black holes. Indeed, there are mounting evidences that the most massive holes at high redshifts power radio–loud AGNs (see, e.g., Ghisellini et al.

2014). These are thought to be associated with Kerr holes – though observational evidences of the widely accepted jet–spin connection are, at best, scarce, even in the well studied Galactic stellar black hole candidates (see, e.g., Russell, Gallo & Fender 2013).

Over the last decade, a number of alternatives to the "light seed scenario" have been proposed. *Heavy* seeds, with masses as large as $\gtrsim 10^4\,\mathrm{M}_\odot$, may form through the direct collapse of low angular momentum gas at high redshifts (see, e.g., Loeb & Rasio 1994; Bromm & Loeb 2003; Koushiappas, Bullock & Dekel 2004; Spaans & Silk 2006; Mayer et al. 2010, 2014), likely via the intermediate stages of a supermassive star and a "quasistar" (Begelman, Volonteri & Rees 2006; Begelman, Rossi & Armitage 2008; Begelman 2010; Dotan, Rossi & Shaviv 2011). For such mechanism to work one needs to, at the same time (i) avoid fragmentation, (ii) effectively dissipate angular momentum, and (iii) drive gas towards the centre of the protogalaxies at a rate $\gtrsim 1\,\mathrm{M}_\odot$ yr^{-1} (e.g, Ferrara, Haardt & Salvaterra 2013; Latif et al. 2015). There is still no consensus, to date, about where and when such conditions are actually fulfilled.

In a previous paper (Madau, Haardt & Dotti 2014, hereinafter MHD14), we discussed super–critical (i.e., super–Eddington) accretion onto stellar mass seeds as a possible mechanism for bypassing the above difficulties. We used the radiatively–inefficient "slim–disc" solution (Abramowicz et al. 1988) – advective, optically thick flows that generalise the standard Shakura & Sunyaev solution (Shakura & Sunyaev 1973) – and showed how mildly super–Eddington accretion significantly eases the problem of assembling MBHs in less than a billion year. Because of the (accretion–rate dependent) low radiative efficiencies of slim discs around non–rotating *as well as* rapidly rotating holes, the accretion time–scale in this regime is almost independent of the spin parameter. It is this unique feature of slim discs that makes such models so appealing.

In MHD14 (see also Volonteri, Silk & Dubus 2015) we briefly discussed how conditions for super–critical accretion are physically plausible in the dense environment of high redshift massive protogalaxies. Here, we elaborate upon this concept by means of high resolution simulations of a cluster of stellar mass black holes orbiting the central ~ 200 pc of a gas–rich galaxy. We show how the interplay between gas dynamics and the black holes can easily lead to the formation of a MBH in the centre of the system within few million years. Though our simulations are highly idealised and should be thought as a proof-of-concept of the scenario we are proposing, they highlight the basic point, i.e. that super–Eddington accretion in well–formed, evolved galaxies is an attractive route to the formation of massive black holes. In fact, a population of stellar mass black holes is expected to reside in the inner ~ 200 pc, the circum–nuclear disc can provide enough gas to be accreted, and negative feedback is negligible in the high–density clumps developed in the disc.

This is the first of a series of papers devoted at the study of the effect of a radiatively inefficient BH feedback on the early growth of stellar mass BHs embedded in a circum–nuclear gas disc. In a forthcoming paper (Fiacconi et al., in preparation) we will discuss the nature and properties of the circum–nuclear gas by means of a fully cosmological, high–resolution simulation of the formation of a gas–rich massive disc galaxy at $z > 6$.

2 SIMULATIONS

We perform a suite of 6 simulations, using the adaptive mesh refinement (AMR) code RAMSES (Teyssier 2002) ("_R" runs) and the new mesh–free code GIZMO (Hopkins 2014) ("_G" runs), which implements a new Lagrangian method to solve the hydrodynamic equations (similar to Godunov–type schemes). The two codes are equipped with similar, but not identical sub-grid recipes for star formation, supernova feedback, BH accretion and BH feedback. While RAMSES is a well-tested AMR code which has been already successfully employed to study circum–nuclear gas discs in merger remnants (Chapon, Mayer & Teyssier 2013), GIZMO employs a novel numerical technique which is in principle well suited to study the flow in a highly dynamical situation while conserving angular momentum and limiting numerical diffusion, with advection errors that are smaller than grid-based cartesian AMR codes such as RAMSES (Hopkins 2014). GIZMO is thus supposed to combine the strengths of grid-based and SPH codes while retaining the tree-based gravity solver inherited from GADGET3, which guarantees high accuracy as well as fast computation for self-gravitating discs like those under study here. The use of two different powerful numerical techniques is aimed at checking the robustness and reproducibility of our results.

2.1 Initial conditions

In our simulations we consider the nuclear region of a high–redshift massive spiral galaxy, where we assume a gaseous circum–nuclear disc (CND hereafter) is hosted. We model the CND following an exponential surface density profile (see Fig. 1, top panel), with total mass $10^8\,\mathrm{M}_\odot$ and scale radius 50 pc. The disc is embedded in a stellar spherical background following an Hernquist profile, with scale radius 100 pc and total mass $2\times10^8\,\mathrm{M}_\odot$. Note that the adopted gas mass from the CND is at the lower end of that of CNDs observed in low z merger remnants (e.g., Medling et al. 2014), and should thus be regarded as a conservative choice for the purpose of our paper. At high redshift galaxies are indeed expected to be more gas rich, which is supported by both theoretical arguments and observational evidence.

The disc, modelled as an ideal gas with polytropic index $\gamma = 5/3$, is set in hydrostatic equilibrium in the global potential with an initial temperature $T = 10^4$ K. The initial conditions are produced using the public code GD_BASIC, described in Lupi, Haardt & Dotti (2015). We show in Fig. 1, bottom panel, the velocity profile of the gas component in the disc. The CND is Toomre unstable since the beginning of the run in the region between 10 pc and 70 pc, as reported in Figure 2 (blue solid line). In order to check if such low temperature could result in overestimated clumpiness we perform two runs of the disc in isolation, one starting with the above mentioned temperature and one with $T = 3\times10^4$ K (the equilibrium temperature in the case of a disc heated by UV background radiation at $z \sim 8$). We do not include UV background radiation in the simulation, assuming the disc will become self–shielded. Despite the initially higher temperature, we find that after only few 10^4 years the disc temperature drops to 7×10^3 K in both runs, converging to an identical profile for the Toomre parameter Q (Figure 2, dashed lines).

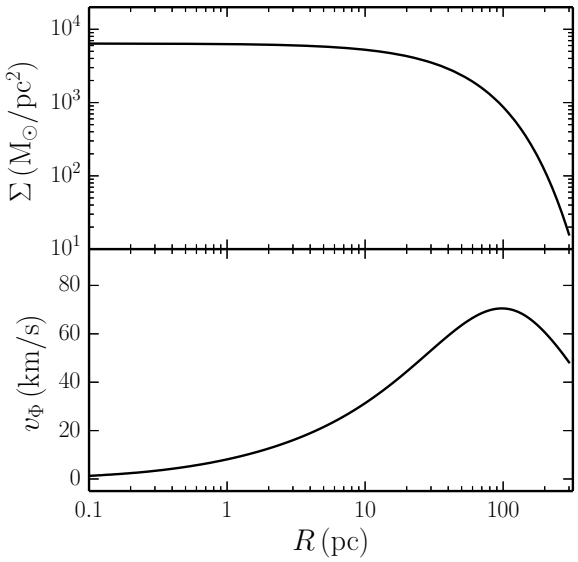

Figure 1. Initial surface density (top panel) and circular velocity (bottom panel) profiles of the circum–nuclear disc.

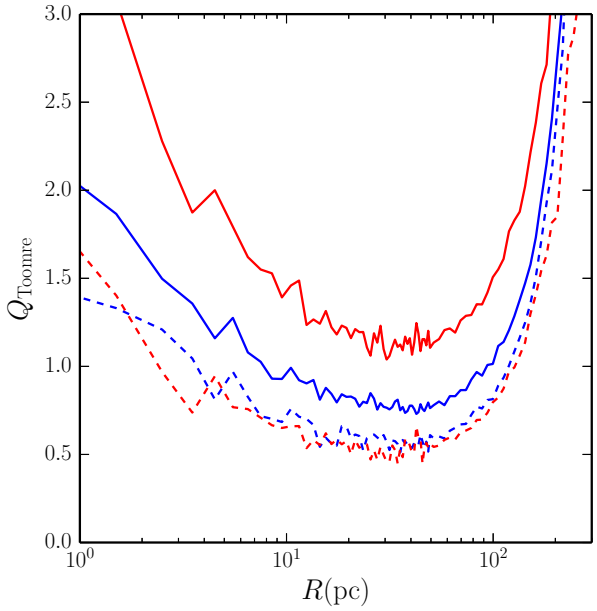

Figure 2. Toomre parameter for the isolated CNDs at $t = 0$ Myr (solid lines) and $t = 0.05$ Myr (dashed lines). The blue line corresponds to an initial temperature $T = 10^4$ K and the red one to an initial temperature $T = 3 \times 10^4$ K.

We then assume that previous star-formation episodes left a population of stellar mass black holes in the galaxy nucleus. The mass of such "black hole seeds" M_{BH} is alternatively set 20 or 100$\mathrm{M}_\odot$. We initially distribute the BHs uniformly within the inner 150 pc of the CND. The BHs lay in the disc plane and have an initial velocity equal to the local circular velocity. We add a randomly oriented velocity component sampled from a normal distribution with standard deviation $\sigma \sim 20\%$ of the maximum circular velocity.

2.2 RAMSES Eulerian simulations

We perform two simulations with RAMSES at two different spatial resolutions, namely 0.4 pc ("low" runs) and 0.1 pc ("med" runs). The mass resolution is $10^3\,\mathrm{M}_\odot$ at the quasi–Lagrangian threshold for refinement. We include the radiative cooling of the gas adopting the standard prescriptions employed in the code (see Teyssier et al. 2013, for details). In order to prevent spurious fragmentation at the highest refinement level we add a polytropic pressure term to the gas component (described as a polytrope with $\gamma = 5/3$ and temperature 10^3 K at $2 \times 10^5\,\mathrm{cm}^{-3}$), ensuring to resolve the Jeans length with at least 4 cells at the highest refinement level.

We set a star formation density and temperature threshold of $\rho_{\mathrm{thr}} = 2 \times 10^5$ cm^{-3} and $T_{\mathrm{thr}} = 2 \times 10^4$ K, and a typical star formation time–scale of 1 Myr. We also assume a time delay between star formation and the corresponding SNa explosion event of 1 Myr, with a SNa yield of 0.15 (corresponding to stars with masses above $8\,\mathrm{M}_\odot$ for a Salpeter IMF). In order to model non thermal processes associated with SNa events, we include the blast–wave like feedback described in Teyssier et al. (2013). In this feedback recipe the SNa energy budget is decoupled from the thermal energy of the gas, preventing, for a typical timescale $\simeq 20$ Myr, the gas to radiatively cool. In our runs we assume a primordial gas composition and we include subsequent metal pollution due to SNae.

2.3 GIZMO Lagrangian simulations

Since the public version of GIZMO only includes basic hydrodynamics and gravity, we implement in the code the additional recipes necessary to model gas cooling, star formation, type II SNa feedback and gas accretion onto BHs, in a fashion similar to RAMSES implementations.

We include radiative cooling by means of the GRACKLE[1] chemistry and cooling library, which provides both equilibrium and non–equilibrium chemistry (The Enzo Collaboration et al. 2014; Kim et al. 2014). In our runs we employ the equilibrium cooling curve for primordial species (atomic H and He), and tabulated metal cooling and heating from Cloudy (Ferland et al. 2013).

Gas particles are eligible for star formation when they match the same criteria for density and temperature adopted in our RAMSES runs and belong to a converging flow (i.e., $\nabla \cdot \mathbf{v} < 0$). Resulting star particles are generated locally according to the Schmidt law (Kennicutt 1998), and using a stochastic prescription as described in Stinson et al. (2006). We model SNa feedback assuming that after a typical timescale of 1 Myr stars above $8\,\mathrm{M}_\odot$ explode as type II SNae, releasing $10^{50}\,\mathrm{erg}/\,\mathrm{M}_\odot$ in the form of purely thermal energy.

The non thermal processes that energise the SNa blast–wave have a typical dissipation timescale much longer than that of the thermal energy. Therefore, we implement a "delayed cooling" prescription as follows: we temporarily inhibit radiative cooling for gas particles within the SNa maximum extension radius R_{E} defined as in Chevalier (1974).

[1] `http://grackle.readthedocs.org`

The SNa energy is then distributed among the gas particles lying within $R_{\rm E}$, according to their distance from the SNa, weighted through the kernel function used in the code. This is different from the approach taken in the RAMSES runs, in which the energy is wholly released within the cell hosting the progenitor. In GIZMO runs we limit the cooling delay time to 5 Myr only (i.e., 4 times smaller than what assumed in our RAMSES runs). We checked that this set up provides consistent results between RAMSES and GIZMO feedback implementations.

We perform three simulations allowing for two different gravitational resolutions, i.e., 0.16 pc ("low" runs) and 0.02 pc ("high" run). We set the same gravitational resolution for gas particles and BH particles. We use 10^5 particles for the "low" runs and 10^7 for the "high" run, corresponding to a mass resolution of $10^3\,{\rm M}_\odot$ and $10\,{\rm M}_\odot$, respectively. In our runs we use the finite mass mode available in the code, in which mass transfer between particles is forbidden, so that our simulations are purely Lagrangian.

2.4 BH accretion

In RAMSES runs we evaluate the accretion onto the stellar mass BHs using the so-called "flux accretion" prescription. In such a scheme the accretion rate is the mass flux rate within the BH accretion zone, which consists of a sphere of radius equal to 4 cells, i.e., $\dot{M}_{\rm acc} = \int -\nabla \cdot [\rho \Delta \mathbf{v}] d^3\mathbf{x}$, where the integral is over the volume of the accretion zone and $\Delta\mathbf{v}$ is the gas–BH relative velocity (see Bleuler & Teyssier 2014, for a detailed description of the implementation).

In order to get a more accurate BH dynamics and to best resolve the accretion rate, we force the region near to each BH to always be at the maximum refinement level, as described in Lupi, Haardt & Dotti (2015). Forcing the resolution close to the BHs at the highest possible level guarantees that nearby cells own a mass $\lesssim 5 \times M_{\rm BH}$ during the whole BH accretion history. This allows us to set $20\,{\rm M}_\odot$ as the initial mass of the BHs in our RAMSES runs.

In GIZMO runs we allow gas accretion onto the stellar–mass BHs for particles lying within a distance from the hole than encompasses an effective number of gas particles $N = 32$. Such *kernel radius* h is therefore implicitly defined through the following relation:

$$\frac{4}{3}\pi h^3 \sum_j W(z_j) = 32. \quad (1)$$

The *volume partition kernel* $W(z_j)$ is a function of the normalised distance to the BH $z_j \equiv |\mathbf{x}_j - \mathbf{x}_{\rm BH}|/h$, where $\mathbf{x}_j$ and $\mathbf{x}_{\rm BH}$ are the position vectors of the j-th gas particle and of the accreting BH, respectively (for further details see Hopkins 2014). Since the kernel radius strongly depends upon the gas density, our scheme would typically overestimate the accretion rate when a BH moves in a low density medium. In order to overcome this problem we enable accretion onto a BH only when the kernel radius is $\leqslant 10$ times the softening length of the sink particle. The accretion rate is then computed as described for RAMSES runs.

Because of the large mass of gas particles the dynamics of BHs as light as 20 ${\rm M}_\odot$ cannot be properly solved for. Therefore, we start from a larger initial BH mass, i.e., $M_{\rm BH} = 100\ {\rm M}_\odot$. With such a choice, BHs in the "high" runs have resolved dynamics since the very beginning of the simulation. In the "low" case, the initial BH dynamics and growth is instead affected by the lack of mass resolution. However, as will be discussed in the next section, some BHs grow above 1000 ${\rm M}_\odot$ in a very short time, making dynamics quickly reliable.

With respect to the standard Bondi-Hoyle model, this recipe does not make any geometrical assumption for the gas flow, allowing for a more accurate estimation of the accretion rate, where the effect of angular momentum on the resolved scales is taken into account. However, despite the high resolution reached with the "high_G" run, we are unable to properly follow the gas from sub–parsec scales down to the accretion disc scale. This resolution limit could result in a overestimated and more efficient accretion. Such a convergence study is beyond the scope of the present work.

2.5 BH feedback

The public release of RAMSES already provides a prescription for AGN thermal feedback (Dubois et al. 2014), in which the radiation produced by accretion is stored until the total budget is large enough to heat up the surrounding gas to at least 10^7 K. This prescription has been initially proposed by Booth & Schaye (2009) to prevent the gas from immediately loose the small amount of additional thermal energy gained after each time–step, which would result in an ineffective feedback. The RAMSES prescription assumes a fixed accretion radiative efficiency $\epsilon = 0.1$, and a fixed fraction $= 15\%$ of the accretion energy to be released to gas. In our simulations we suitably modify this recipe to include the effects of accretion in the fashion of slim disc (Sądowski et al. 2014). To this aim, we estimate ϵ using the analytical fit to the numerical results by Sądowski et al. (2014) provided by Madau, Haardt & Dotti (2014):

$$\epsilon = \frac{r}{16} A(a) \left[\frac{0.985}{r + B(a)} + \frac{0.015}{r + C(a)} \right], \quad (2)$$

where $r = \dot{M}_{\rm E}/\dot{M}$. Here $\dot{M}_{\rm E} = 16 L_{\rm E}/c^2$ where $L_{\rm E}$ is the Eddington luminosity. A, B, C are fitting functions scaling with the BH spin a as

$$A(a) = (0.9663 - 0.9292a)^{-0.5639}, \quad (3)$$
$$B(a) = (4.627 - 4.445a)^{-0.5524}, \quad (4)$$
$$C(a) = (827.3 - 718.1a)^{-0.7060}. \quad (5)$$

At each accretion event we compute the released energy allowed to feedback on nearby particles using this new value for ϵ instead of the fixed value 0.1, while the spin is always fixed at $a = 0.99$ for all BHs. We implement in GIZMO the same prescription for BH feedback. In all simulations we do not include other possible forms of BH feedback, e.g., momentum-driven.

Finally, in order to check whether super–critical accretion is instrumental in leading to very large $M_{\rm BH}$ in a short time, we perform two GIZMO runs setting the radiative efficiency to its custom value, $\epsilon = 0.1$ (low_G_0.1 and high_G_0.1 runs). We report the details of our six simulations in table 1.

Run	Resolution (pc)	BH mass ($M_\odot$)	Accretion radius (pc)	ϵ
low_R	0.40	20	1.6	Slim
med_R	0.10	20	0.4	Slim
low_G	0.16	100	< 1.6	Slim
high_G	0.02	100	< 0.2	Slim
low_G_0.1	0.16	100	< 1.6	0.1
high_G_0.1	0.02	100	< 0.2	0.1

Table 1. Settings of our simulation suite. The second column reports the gravitational resolution (for _G runs) and the highest refinement level resolution (for _R runs). The fourth column is the accretion radius, which is fixed to 4 cells for _R runs and depends on the smoothing length for _G runs. The last column indicates the type of accretion recipe used.

3 RESULTS

Figure 3 shows the comparison between the low resolution GIZMO runs with (low_G) and without (low_G_0.1) the slim disc implementation. All the other simulation parameters are the same in the two simulations. It is immediately clear from the comparison that whenever a BH undergoes an intense accretion episode, the large feedback energy available in the radiatively efficient low_G_0.1 case evacuates the BH surroundings, efficiently limiting further BH growth. In the low_G case, on the contrary, even accretion rates significantly higher than $\dot{M}_{\rm E}$ result in moderate luminosities that do not impact on the densest gas clumps, and therefore BHs can grow considerably faster. As an example, in the low_G run the most mass growing BH (that will be referred to as $\rm BH_{top}$ in all runs hereafter, red line in the bottom–left panel of figure 3) reaches a mass larger by up to 2 order of magnitudes compared to the corresponding $\rm BH_{top}$ in the radiative efficient case at the end of the simulation (red line in the top–left panel panel). The low radiative efficiency of slim discs has then a double effect: first, for any given accretion rate BHs grow faster simply because less mass is lost as radiation (the "$(1-\epsilon)$-effect"); second, the reduced radiative efficiency results in a reduced feedback on the accreting gas, and larger accretion rates are therefore possible (the "$\dot{M}$-effect").

In order to asses how numerical resolution affects our results, we analyse the two high resolution GIZMO runs (high_G and high_G_0.1), and compare the outputs to the low resolution cases discussed above. Figure 4 shows the accretion history of BHs (left panels) and the effect the accretion feedback has on the gas (right panels). Because of the higher resolution we can now resolve a smaller accretion region around each BH, which has the net effect of reducing the BH mass growth compared to the corresponding low resolution runs. Nevertheless, it is apparent how, also in these high resolution simulations, BH mass growth is strongly suppressed in the radiatively efficient case (top panels). Indeed, for $\epsilon = 0.1$, $\rm BH_{top}$ increases its mass by only $\simeq 50\%$ of its initial value. We stress again that the different radiative efficiency is only marginally responsible of the different accreted mass in the two cases. As clearly shown in the right panels of Figure 4, the largest effect is played by the accretion feedback that, in the standard high-efficiency case, evacuates the region closer to the BHs, hence inhibiting further gas accretion.

The implementation of a physically motivated radiative inefficient accretion mode is then a necessary condition for a fast, highly super–Eddington growth of BHs in our simulations, but, as we will show next, is not sufficient. In the following we will focus only on runs including the slim disc prescription, in order to link episodes of super–Eddington growth with the physical state of the BHs and of the nuclear disc, with the ultimate aim of understanding the processes that can possibly lead to high accretion rates.

Figure 5 shows the results of the highest resolution RAMSES run med_R. The upper left panel reports the mass evolution of the 20 BHs as a function of time. As for the low_G simulation discussed above, the implementation of the slim disc efficiency prescription allows $\rm BH_{top}$ (shown as a red line) to grow within 3 Myr by up to ~ 3 orders of magnitude in mass. Note that $\rm BH_{top}$ is not necessary the earliest growing BH of the cluster.

The upper right panel of figure 5 focuses on $\rm BH_{top}$ alone, showing the time evolution of the accretion rate, and the corresponding distance from the gas clump the BH bounds to during the peak of its mass growth. The accreting clump forms out of a spiral stream developing in the cooling disc, and can not be clearly identified as a bound structure before $t \approx 1$ Myr, as shown in the middle left panel. $\rm BH_{top}$ passes a first time through the overdense stream (middle right panel), and experiences a short $\lesssim 0.1$ Myr super–Eddington accretion episode, but the radial component of its velocity quickly is large enough to displace it from the overdensity (as observed in the $\dot{m}_{\rm BH}$ plot, upper right panel). As the clump grows in mass (up to a maximum of $\sim 3 \times 10^4\,M_\odot$ in gas), the $\rm BH_{top}$ feels its gravitational attraction, and is eventually captured by the clump. At this time $\rm BH_{top}$ undergoes a longer (~ 0.5 Myr) intense super–Eddington accretion phase. Being the initially small BH surrounded by an overwhelmingly large and cold gas cloud, the BH accretes at the maximum rate allowed by the code (i.e. $500 \times \dot{M}_{\rm E}$) until almost all gas is turned into stars. At this point $\rm BH_{top}$ (already grown by 3 order of magnitudes in mass), together with stars exploding as SNae, can evacuate the residual gas condensation (lower right panel). Note that BHs (including $\rm BH_{top}$) accrete most of their mass from, essentially, a single dense clump they randomly come across during the dynamical evolution of the system.

It is important to realise that the gravitational capture of a BH by a dense gas clump is intrinsically stochastic, as clumps form in the disc via gravitational instabilities of cooling gas independently of the presence of seed holes. While the BH–capture process is common in all the simu-

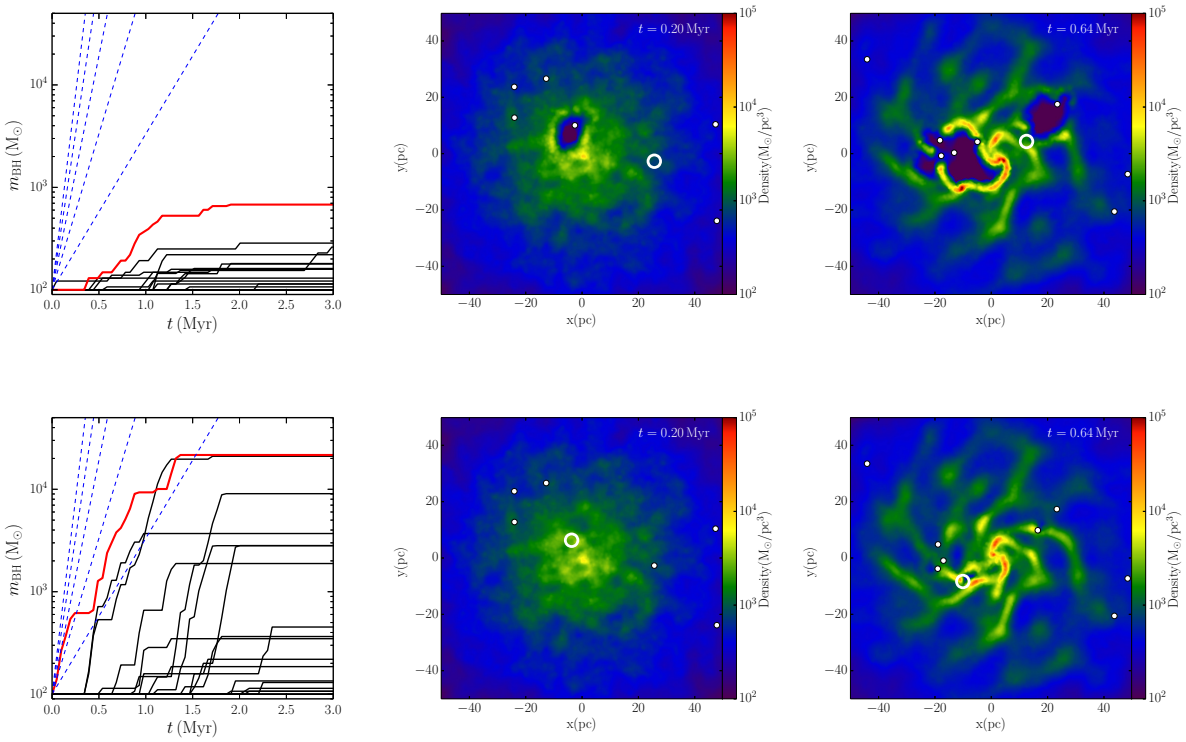

Figure 3. Left panels: BH masses as a function of time for runs low_G_0.1 (top panel) and low_G (bottom panel). The red lines correspond to the most massive BHs ($\rm BH_{top}$) at the end of the runs, while the blue dashed lines trace accretion histories at fixed Eddington ratios of 500, 400, 300, 200 and 100, respectively. Central and right panels: gas density maps for the two runs at $t = 0.2$ and 0.64 Myr, respectively. The white dots mark the positions of the BHs.

lations we ran, the number and mass distributions of gas clumps and, consequently, the fraction of BHs that bind to them, in fact depend upon the spatial and mass resolution we achieve. Figure 6 shows a comparison between runs with different spatial resolution. Among the runs including the slim disc implementation, only run med_R (already shown in Figure 5) is left out of the direct comparison.

A first clear difference is observable at early times. The runs with lower resolution show a faster initial growth of each individual BH, and the number of growing BHs right after the beginning of the runs ($t \lesssim 0.5$ Myr) also increases with decreasing resolution. These trends are caused by the larger accretion radius implemented in the lower resolution runs. In these simulations the BHs can start accreting well before the disc develops any significant overdensity. For this reason the feedback of the early BH accretion onto the gas is more efficient, as a larger energy is injected in a lower density medium. As the resolution increases and the accretion radius can be decreased, fewer BHs have an early start, as in the med_R run (upper left panel of Figure 5) and, more evidently, in the high_G run (lower left panel of Figure 6).

The high_G run, thanks to the exquisite mass and spatial resolutions achieved, shows a richness of structures observable directly in the density map (see the lower right panel of Figure 6 in particular), in which the formation of dense clumps as well as the feedback exerted by the ongoing SF are clearly visible. The gas particles tracing the gas evolution allow us to follow the formation of the massive clump from which $\rm BH_{top}$ gains its mass. Figure 8 reports two different projections of $\rm BH_{top}$ orbit along with the trajectories of 50 gas particles randomly extracted from those forming the massive clump $\rm BH_{top}$ binds to and accretes from. The clump formation clearly proceeds out of a gas gravitational instability within the dense disc, and starts interacting with $\rm BH_{top}$ only when their orbits intersect. Strong gravitational perturbations to the BH orbit are clearly seen when the two systems bind gravitationally. The BH growth then exerts a feedback onto the gas particles, that, together with stars exploding as SNae, results in a partial ejection of particles from the BH neighbourhoods and out of the disc plane (as clearly see in Figure 8 lower panel).

We finally analyse the physical properties of clumps in the high_G run using the public tool SKID[2], and report our results for both the disc-like clumps and the more extended gravitationally bound streams in table 2. Clump properties are evaluated at $t \sim 1.6$ Myr, when $BH_{\rm top}$ is in its main accretion phase. Fig. 7 shows the clumps in the disc density map. The reported circular velocity is computed at the half mass radius of the clump. It is worth noticing that typical masses (ranging from few $10^2\,{\rm M}_\odot$ up to few $10^5\,{\rm M}_\odot$), as well as the density of our clumps are compatible with the observed properties of local giant molecular clouds (GMCs), though the latter are much less compact (Lombardi, Alves &

[2] `https://github.com/N-BodyShop/skid`

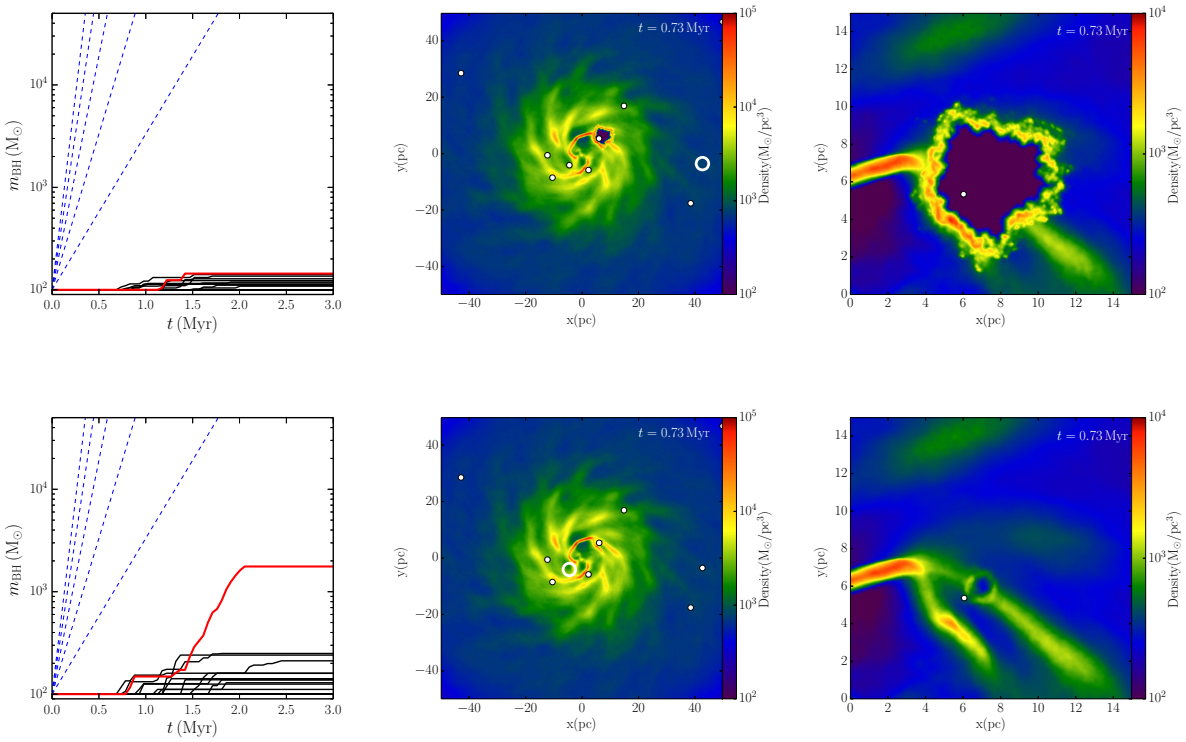

Figure 4. Left panels: BH masses as a function of time for runs high_G_0.1 (top panel) and high_G (bottom panel). The red lines correspond to the most massive BHs ($\rm BH_{top}$) at the end of the runs, while the blue dashed lines trace accretion histories at fixed Eddington ratios of 500, 400, 300, 200 and 100, respectively. Central panels: gas density maps for the two runs at $t = 0.73$ Myr. Right panels: zoom in of a region heated by BH feedback. The white dots mark the positions of the BHs.

Lada 2010). The average temperature of the clumps is much higher than the typical temperature of GMCs, mainly because we neglected molecular hydrogen cooling and, at the same time, the metal production in the few Myr of our simulations is not sufficient to significantly alter the gas cooling function. While allowing for a more efficient cooling would initially boost SF in the clumps, further SF could be hampered by the enhanced UV dissociating flux [3].

We conclude by noticing that in our idealised runs the growth of the BHs is finally halted by the star formation–driven gas consumption, and by gas ejection triggered by SNae. However, in a cosmological perspective, the galaxy nucleus would be replenished of gas coming from large scale filaments and/or galaxy mergers. The very short duration of the super–Eddington accretion bursts allows for the growth of stellar mass BHs up to $\gtrsim 10^4\,{\rm M}_\odot$ or more on a time comparable (or even shorter) than the star–formation timescale.

[3] We can speculate that, if clumps become self-shielded to dissociating radiation and SF continues unimpeded, dense stellar systems could form, which eventually might be prone to dynamical instabilities. A detailed analysis of the formation of dense stellar clusters in our simulations is beyond the scope of the current study.

4 DISCUSSION AND CONCLUSIONS

We presented the results from a suite of numerical high resolution simulations aimed at studying the accretion of stellar mass BHs in nuclear gaseous discs. We implemented a new BH thermal feedback prescription, that takes into account the possible occurrence of radiatively inefficient accretion bursts during which the BHs can actually increase their masses at a significantly super–Eddington pace. We have employed both AMR and Lagrangian mesh-free simulations, achieving comparable results, which strengthens greatly our conclusions.

The set up of our runs is highly idealised, since BHs are supposed to be already in place in a well formed gaseous disc. The latter, at the beginning of the simulation, starts cooling and eventually forms stars. Furthermore, our simulations are evolved in complete isolation, i.e., no gas flows into the nuclear disc from larger scales (e.g., from outer regions of the host galaxy, from cosmological filaments, or through galaxy mergers). As a consequence, every accretion episode halts when star formation and SNa–driven gas consumption have evacuated the central disc regions.

Though the prescriptions adopted in our simulations regarding star formation and SNa feedback could, in principle, affect the growth of BHs, they are conservative for what concerns gas accretion onto the BHs. First, the star formation rate in a sphere of radius $\simeq 1$ pc (corresponding to the average clump radius) around $\rm BH_{top}$ is $\simeq 0.1\,{\rm M}_\odot$/yr, much

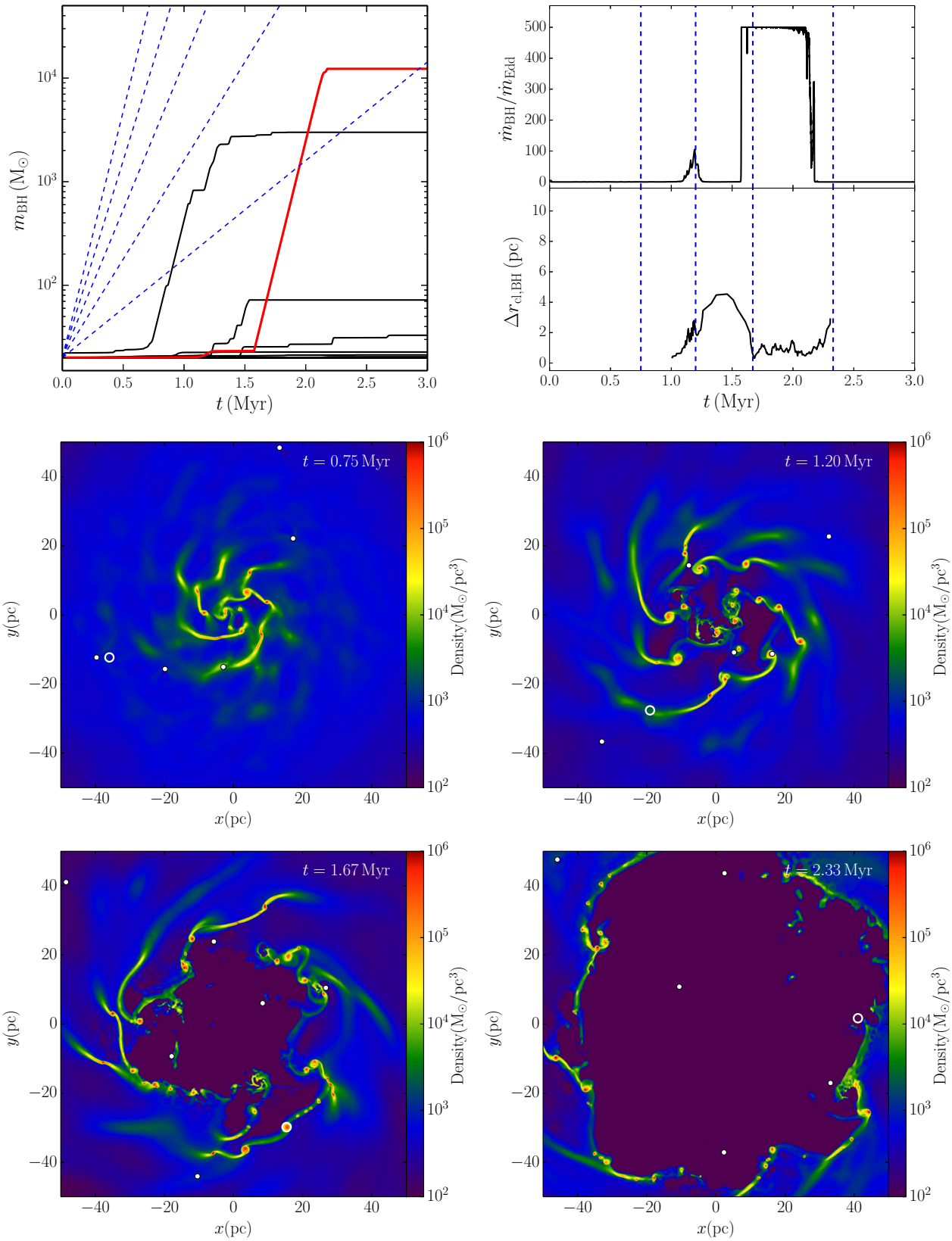

Figure 5. Run med_R. Upper left panel: BH masses vs time for all the 20 BHs. The dashed lines show the slope of accretion episodes at 500, 400, 300, 200 and 100 $\dot{M}_{\rm E}$. Upper right panel: accretion rate for BH$_{\rm top}$, and distance from the clump BH$_{\rm top}$ bounds to during the peak of its mass growth. Middle and lower panels show the density in the equatorial disc plane of the gas at $t = 0.75$, 1.2, 1.67 and 2.33 Myr (corresponding to the times highlighted by the dotted lines in the upper upper right panel). The BH$_{\rm top}$ is reported as large white ring, while the other BHs are shown as smaller white dots.

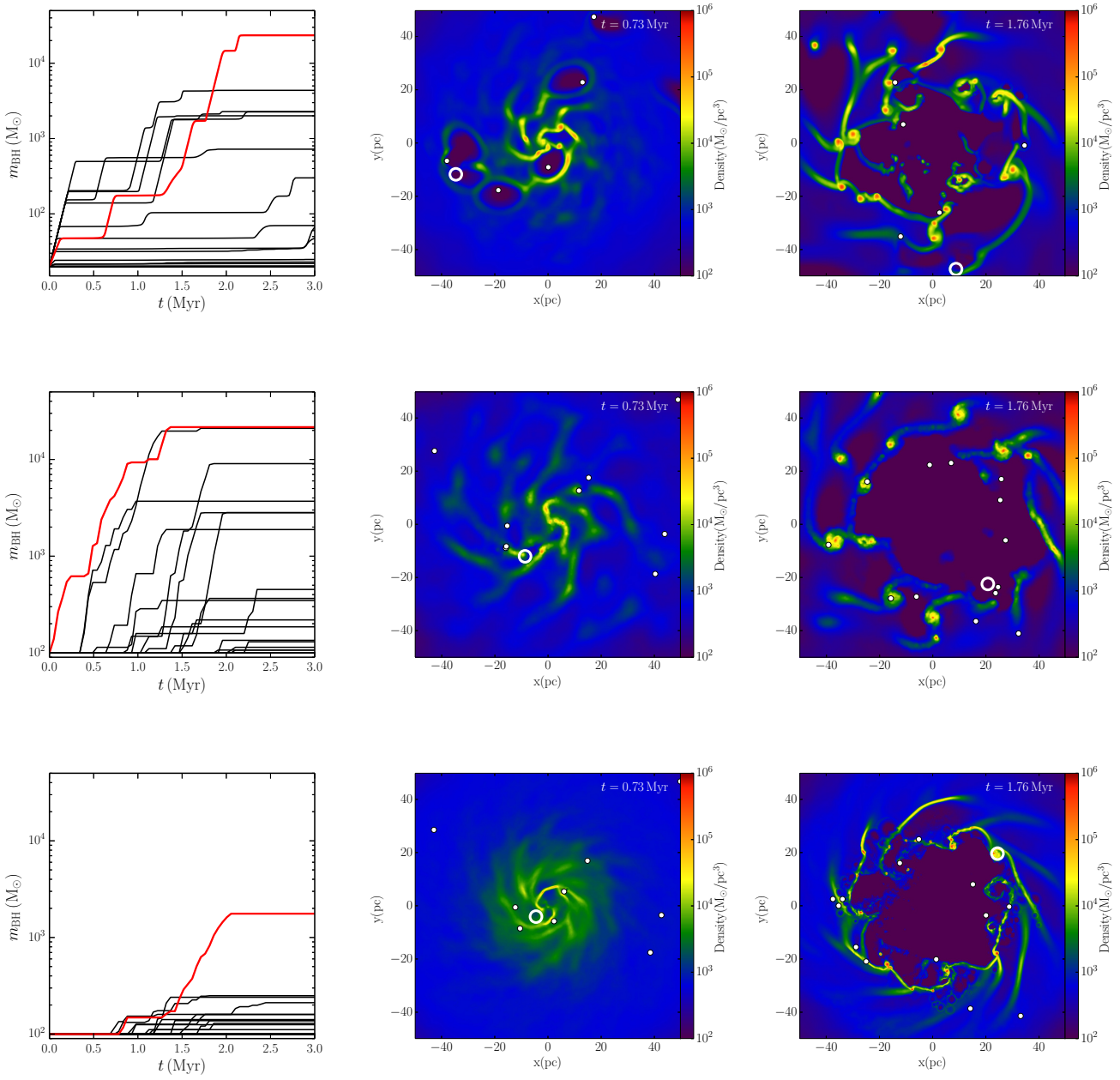

Figure 6. Upper panels: Mass as a function of time of the BHs (left panel), gas density at $t = 0.73$ Myr (central panel) and $t = 1.76$ Myr for the low_R run. The positions of the BHs are shown as white dots. The growth of $\rm BH_{top}$ is highlighted in the left panel with a red line, and its position in the central and right panels is marked with a large white ring. Middle and lower panels, the same as the upper panels for run low_G and high_G, respectively.

larger than the average BH accretion rate ($\simeq 10^{-3}\,\rm M_\odot/yr$). Hence, we can be confident that in our simulations the gas is mostly consumed by star formation rather than by BH accretion. To further prove the point we run a low resolution GIZMO simulation in which we increase the star formation efficiency to its maximum value, and find that even for the resulting extremely high star formation rate ($\sim 40\,\rm M_\odot/yr$) the BH accretion history is not significantly modified. Second, our assumed timescale for SNa explosions (1 Myr) is shorter than the typical lifetime of low metallicity stars in the mass range $8 - 40\,\rm M_\odot$ ($\gtrsim 4$ Myr; Hurley, Pols & Tout (2000)). Our resulting SNa feedback is then already very highly efficient[4]. In this context, we find that SNe produce a high velocity wind ($v_{\rm ej} \lesssim 3000\,\rm km/s$), which can expand

[4] We run a further GIZMO low resolution simulation and checked that only an unrealistic "maximally efficient" SNa feedback (in which stars explode as soon as they form) is able to evacuate the gas from the centre before the stellar-size BHs can start to accrete.

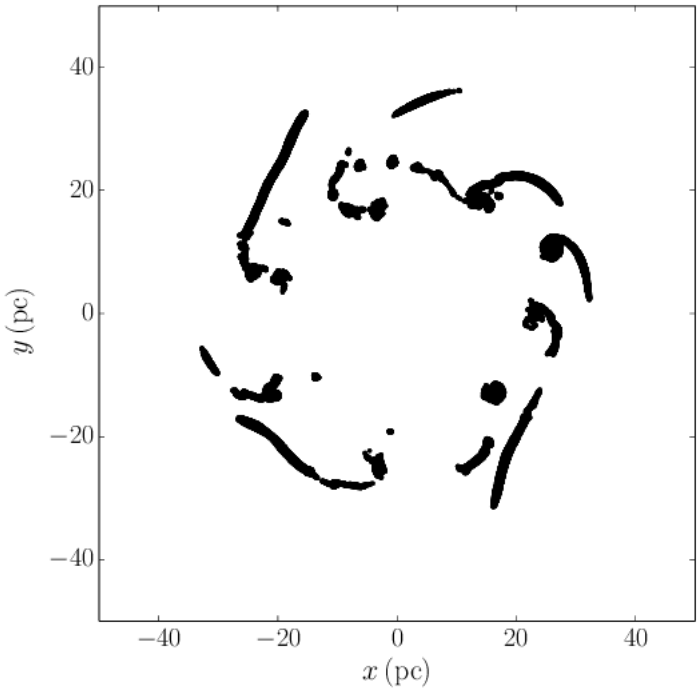

Figure 7. Map of clumps in the high_G run at $t \sim 1.6$ Myr. The clumps can be grouped in two different classes: CL exhibit a disc-like shape and BS are extended bound streams.

M^a	$R^b_{1/2}$	$v^c_{1/2}$	T^d	ρ^e
Bound clumps				
8.70×10^2	0.21	2.98	8.77×10^3	6.77×10^5
1.80×10^3	0.31	3.51	8.89×10^3	7.06×10^5
2.53×10^3	0.24	4.77	8.65×10^3	7.73×10^5
1.68×10^4	0.16	14.96	9.94×10^4	2.26×10^7
3.21×10^4	0.28	15.85	2.91×10^4	5.94×10^6
5.58×10^4	2.48	6.95	1.64×10^4	2.71×10^6
6.75×10^4	0.27	23.22	5.78×10^4	1.31×10^7
8.05×10^4	0.48	18.98	3.47×10^4	7.04×10^6
8.87×10^4	0.48	20.04	2.95×10^4	5.73×10^6
9.38×10^4	0.41	22.27	4.12×10^4	8.40×10^6
1.24×10^5	0.91	17.07	2.23×10^4	4.09×10^6
1.60×10^5	0.70	22.14	3.96×10^4	8.18×10^6
2.14×10^5	1.66	16.64	1.55×10^4	2.51×10^6
Bound streams				
1.13×10^4	0.89	5.24	8.24×10^3	5.45×10^5
3.51×10^4	1.59	6.89	8.43×10^3	5.63×10^5
8.28×10^4	2.55	8.36	2.28×10^4	2.48×10^6
1.70×10^5	3.48	10.24	9.31×10^3	8.05×10^5
1.73×10^5	1.85	14.16	2.41×10^4	4.60×10^6
2.15×10^5	1.16	20.02	3.60×10^4	7.54×10^6
3.25×10^5	7.00	9.99	1.92×10^4	3.30×10^6
3.90×10^5	5.36	12.51	1.20×10^4	1.53×10^6
4.83×10^5	2.91	18.91	1.90×10^4	3.29×10^6

Table 2. Properties of the clumps in the high_G simulation at $t \sim 1.6$ Myr. The bound structures with an almost spherical shape have been classified as bound clumps, while the most asymmetric ones have been classified as bound streams. ^{a} : clump mass in solar masses. ^{b} : clump half mass radius in pc. ^{c} : circular velocity at half mass radius in km/s. ^{d} : gas mean temperatures in K. ^{e} : gas mean number density in cm^{-3}.

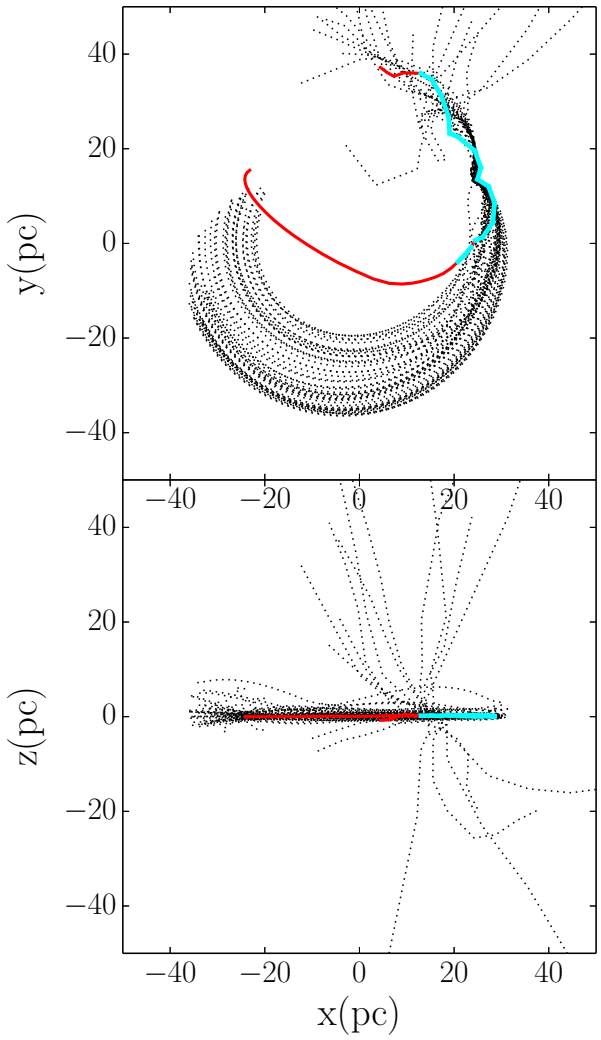

Figure 8. Solid red lines show the face–on (top panel) and edge–on (bottom panel) projections of the trajectory of BH_{top} in run high_G. Black dotted lines trace the orbits of a sample of the gas particles forming the gas clump BH_{top} binds to. The accretion burst due to the BH_{top}–clump interaction is highlighted in cyan.

up to 5 kpc above the disc plane. In principle such gas could form a galactic fountain falling back on to the disc, allowing for a new phase of super-critical accretion.

The cooling function employed in our simulations does not take into account molecular hydrogen, which could induce stronger fragmentation in the disc, and enhance SF. This could, in principle, limit the accretion on to the BHs. However, the presence of radiative feedback from stars (not considered in this study) would act in the opposite direction, dissociating molecular hydrogen and thus allowing for higher inflow rates towards the BHs. Both the modelling of the large scale galactic potential (essential to assess the fate of the SNa driven wind) and the effect of molecular hydrogen cooling (and related stellar dissociating flux) are beyond the scope of our study.

Regardless the spatial/mass resolution and the kind of hydrodynamical code used, a coherent picture emerges. If BHs have to grow by 2-3 order of magnitudes in mass, radiative inefficient accretion is a necessary condition, but not a sufficient one. BHs must find themselves embedded in gas structures that need to be: (i) massive enough to provide the gas reservoir, and (ii) dense enough to survive feedback. This may occur when the cooling gas fragments in clumps, and some of the BHs bind to them. Such process allows some of the BHs to reach masses as high as 10^3 - 10^4 $M_\odot$ on Myr timescales, making them viable candidates as seeds of the supermassive variety of BHs powering high redshift quasars.

Mass accretion onto the BHs depends upon the number, mass and density of the clumps forming in the disc. We showed that these parameters are affected by the numerical resolution achieved in the different runs and, as discussed in Section 3, different resolutions result in different BH accretion histories. We are unable to describe gas dynamics down to the accretion disc scales, even at the highest spatial resolution reached, and this limits our ability to achieve firm estimates of accretion rate and mass growth of the BHs. Yet, the dynamics of gas leading to the formation of dense clouds we observe in all our runs is strongly independent of sub–grid recipes. The gas within the accretion radius of BHs is far from being rotationally supported. Since the relative gas-BH velocity becomes negligible after the capture process, the gas in fact experiences almost radial inflow toward the BHs. Our estimate of the accretion rate is of the same order of the Bondi accretion rate given the temperature and density of the medium surrounding the BHs.

Therefore, despite our accretion histories are not accurate enough from a quantitative point of view, we can be confident about the reliability of the BH-clumps-capture process we observe. Our work should be considered as a *proof of concept*, robust enough to understand under which conditions and through which processes a cluster of stellar mass BHs can actually experience episodes of super–Eddington growth, and what are the effects on the environment.

We conclude that a radiatively inefficient accretion, together with the aforementioned BH-clumps-capture process, can result in mass growths 10-100 times larger than in the radiatively efficient case, making this mechanism a viable candidate to grow massive BH seeds from stellar mass BHs.

The process we studied can result in a prolonged super–Eddington accretion phase only as long as the masses of the clumps are comparable or larger than the masses of the accreting BHs. While the gravitational capture itself easily binds small clumps to comparatively massive BHs, the available gas reservoir is not sufficient for significant BH growth. Moreover, even feedback from radiative inefficient accretion severely affects such small clumps.

Other feedback processes, e.g., momentum-driven feedback, might be important, and will be explored in the future. If, however, such processes turn out to be inefficient, this could naturally allow the galaxy to remain highly star–forming despite the fast growth of the MBH, perhaps explaining the new puzzling observation of a high-z star forming galaxy hosting an SMBH well overweight for its stellar mass (Trakhtenbrot et al. 2015).

In addition, as soon as a BH becomes significantly heavier than typical gas clumps, it starts migrating toward the centre of the disc via dynamical friction. This process will naturally bring the most massive BH (the one that by chance had the largest mass growth, i.e., BH_{top}) to the centre of the host galaxy, where MBHs are commonly observed. At this

point, however, further clumps forming in the disc no longer interact with the central BH.

In order for the large nuclear gas reservoir assumed in our initial conditions to be present in the galactic nucleus disc angular momentum needs to be removed well before gas turns into stars, so that inflowing material can be, at least partially, accreted by the central BH. This is of course the longstanding fuelling problem of MBH debated in the community (e.g., Hicks et al. 2013, and references therein), and its discussion is beyond the goal of the present study. Paper II will deal with the nuclear properties and gas inflows in a galaxy at $z \sim 6-10$ which by $z = 3$ will have a mass comparable to that of the observed clumpy star forming discs, thus allowing to place our model more properly in the context of galaxy formation and test its assumptions and outcomes. Preliminary analysis shows that the mass enclosed within a hundred pc scale fluctuates between a few times $10^7 M_\odot$ and just above $10^8 M_\odot$. So, as mentioned in Section 2, our initial conditions seem to be well motivated.

We finally note that, whenever inflowing gas refills the circum–nuclear disc, the whole process we simulated is rejuvenated: a new massive BH seed will be formed, sinking to the centre of the galaxy and eventually forming an intermediate massive black hole binary bound to coalesce owing to gravitational radiation losses. This kind of systems may be a perfect target for the planned eLISA observatory (Amaro-Seoane et al. 2013).

5 ACKNOWLEDGEMENTS

We thank the anonymous referee for his/her comments and suggestions that helped us to improve the quality of the paper. AL, FH and MD acknowledge financial support from the Italian MIUR, through PRIN 2010-2011. Simulations were run on the EURORA cluster at CINECA and on the Lucia cluster at DiSAT, University of Insubria. P.M. acknowledges support by the NSF through grant AST-1229745 and NASA through grant NNX12AF87G.

REFERENCES

Abramowicz M. A., Czerny B., Lasota J. P., Szuszkiewicz E., 1988, ApJ, 332, 646
Alvarez M. A., Wise J. H., Abel T., 2009, ApJ, 701, L133
Amaro-Seoane P. et al., 2013, GW Notes, Vol. 6, p. 4-110, 6, 4
Begelman M. C., 2010, MNRAS, 402, 673
Begelman M. C., Rossi E. M., Armitage P. J., 2008, MNRAS, 387, 1649
Begelman M. C., Volonteri M., Rees M. J., 2006, MNRAS, 370, 289
Bleuler A., Teyssier R., 2014, MNRAS, 445, 4015
Booth C. M., Schaye J., 2009, MNRAS, 398, 53
Bromm V., Loeb A., 2003, ApJ, 596, 34
Chapon D., Mayer L., Teyssier R., 2013, MNRAS, 429, 3114
Chevalier R. A., 1974, ApJ, 188, 501
Dotan C., Rossi E. M., Shaviv N. J., 2011, MNRAS, 417, 3035
Dubois Y., Volonteri M., Silk J., Devriendt J., Slyz A., 2014, MNRAS, 440, 2333
Fan X. et al., 2006, AJ, 131, 1203
Ferland G. J. et al., 2013, Rev. Mexicana Astron. Astrofis., 49, 137
Ferrara A., Haardt F., Salvaterra R., 2013, MNRAS, 434, 2600
Ghisellini G., Celotti A., Tavecchio F., Haardt F., Sbarrato T., 2014, MNRAS, 438, 2694
Haiman Z., Loeb A., 2001, ApJ, 552, 459
Heger A., Fryer C. L., Woosley S. E., Langer N., Hartmann D. H., 2003, ApJ, 591, 288
Hicks E. K. S., Davies R. I., Maciejewski W., Emsellem E., Malkan M. A., Dumas G., Müller-Sánchez F., Rivers A., 2013, ApJ, 768, 107
Hopkins P. F., 2014, ArXiv e-prints, 1409.7395
Hurley J. R., Pols O. R., Tout C. A., 2000, MNRAS, 315, 543
Kennicutt, Jr. R. C., 1998, ApJ, 498, 541
Kim J.-h. et al., 2014, ApJS, 210, 14
Koushiappas S. M., Bullock J. S., Dekel A., 2004, MNRAS, 354, 292
Latif M. A., Bovino S., Grassi T., Schleicher D. R. G., Spaans M., 2015, MNRAS, 446, 3163
Loeb A., Rasio F. A., 1994, ApJ, 432, 52
Lombardi M., Alves J., Lada C. J., 2010, A&A, 519, L7
Lupi A., Haardt F., Dotti M., 2015, MNRAS, 446, 1765
Madau P., Haardt F., Dotti M., 2014, ApJ, 784, L38
Madau P., Rees M. J., 2001, ApJ, 551, L27
Madau P., Rees M. J., Volonteri M., Haardt F., Oh S. P., 2004, ApJ, 604, 484
Mayer L., Fiacconi D., Bonoli S., Quinn T., Roskar R., Shen S., Wadsley J., 2014, ArXiv e-prints, 1411.5683
Mayer L., Kazantzidis S., Escala A., Callegari S., 2010, Nature, 466, 1082
Medling A. M. et al., 2014, ApJ, 784, 70
Milosavljević M., Bromm V., Couch S. M., Oh S. P., 2009, ApJ, 698, 766
Mortlock D. J. et al., 2011, Nature, 474, 616
Russell D. M., Gallo E., Fender R. P., 2013, MNRAS, 431, 405
Sądowski A., Narayan R., McKinney J. C., Tchekhovskoy A., 2014, MNRAS, 439, 503
Shakura N. I., Sunyaev R. A., 1973, A&A, 24, 337
Spaans M., Silk J., 2006, ApJ, 652, 902
Stinson G., Seth A., Katz N., Wadsley J., Governato F., Quinn T., 2006, MNRAS, 373, 1074
Tanaka T., Haiman Z., 2009, ApJ, 696, 1798
Teyssier R., 2002, A&A, 385, 337
Teyssier R., Pontzen A., Dubois Y., Read J. I., 2013, MNRAS, 429, 3068
The Enzo Collaboration, Bryan G. L. et al., 2014, ApJS, 211, 19
Trakhtenbrot B. et al., 2015, Science, 349, 168
Volonteri M., Haardt F., Madau P., 2003, ApJ, 582, 559
Volonteri M., Silk J., Dubus G., 2015, ApJ, 804, 148
Wise J. H., Turk M. J., Abel T., 2008, ApJ, 682, 745